Cauchy-Rician Model for Backscattering in Urban SAR Images

Oktay Karakuş, *Member, IEEE,* Ercan E. Kuruoğlu, *Senior Member, IEEE,* Alin Achim, *Senior Member, IEEE,* Mustafa A. Altınkaya, *Member, IEEE,*

***Abstract*—This letter presents a new statistical model for modelling urban scene SAR images by combining the Cauchy distribution, which is heavy tailed, with the Rician back-scattering. The literature spans various well-known models most of which are derived under the assumption that the scene consists of multitudes of random reflectors. This idea specifically fails for urban scenes since they accommodate a heterogeneous collection of strong scatterers such as buildings, cars, wall corners. Moreover, when it comes to analysing their statistical behaviour, due to these strong reflectors, urban scenes include a high number of high amplitude samples, which implies that urban scenes are mostly heavy-tailed. The proposed Cauchy-Rician model contributes to the literature by leveraging non-zero location (Rician) heavy-tailed (Cauchy) signal components. In the experimental analysis, the Cauchy-Rician model is investigated in comparison to state-of-the-art statistical models that include $\mathcal{G}_0$, generalized gamma, and the lognormal distribution. The numerical analysis demonstrates the superior performance and flexibility of the proposed distribution for modelling urban scenes.**

***Index Terms*—Urban modelling, SAR Imaging, Cauchy-Rician distribution.**

I. Introduction

THIS letter concerns with the statistical modelling of urban areas in synthetic aperture radar (SAR) imagery, which are mostly characterised by a high number of strong scatterers caused by the man-made structures with dihedral or trihedral configurations [1]. Especially, for SAR application areas of classification, denoising and segmentation to utilise an advanced and accurate statistical model leads to better performances.

The standard model for the back-scattered SAR signal from a given area, exploits a complex signal, with a form of $R = x_1 + jx_2$ [2], [3]. The SAR literature abounds with multitude of statistical models which are either based on the physics of the imaging process or empirical. The simplest model for SAR amplitude assumes the real (x_1) and imaginary (x_2) parts are independent and identically distributed (i.i.d.) zero-mean Gaussian random variables. This leads SAR distribution for the amplitude $r = \sqrt{x_1^2 + x_2^2}$ to become the Rayleigh model which is valid provided there is no dominating scatterer in the scene. When the Rayleigh model is not the case whilst having various dominating scatterers, the real and imaginary signal components become non-zero mean ($\delta \neq 0$) Gaussian, which hence lead amplitude distribution to become the Rician distribution,

$$f(r|\gamma, \Delta) = \frac{r}{\sigma^2} \exp\left(-\frac{r^2 + \Delta^2}{2\sigma^2}\right) \mathcal{I}_0\left(\frac{r\Delta}{\sigma^2}\right) \qquad (1)$$

where $\Delta = \sqrt{2}\delta$ is the location parameter and $\mathcal{I}_0(\cdot)$ refers to the zeroth-order modified Bessel function of the first kind. Rician model is widely used to characterise SAR scenes containing many strong back-scattered echoes. These include natural targets such as forest canopy, mountain tops, sea waves, as well as some man-made structures with dihedral or trihedral configurations such as cars, buildings, or vessels [1], [4]–[7].

Notwithstanding their appealing theoretical properties, and simple analytical structure, statistical models based on the Gaussian assumption (Rayleigh-Rician) do not reflect the real life phenomena in most cases for SAR reflections which exhibit impulsive behaviour indicative of underlying heavy-tailed distributions. Thus, there are numerous statistical models in the literature which were developed to account for non-Rayleigh cases, and proven to be successful for modeling SAR imagery. A non-exhaustive list of models can be given as: Gamma [8], [9], Weibull [10], [11], lognormal [12], $\mathcal{K}$ [8], [13], $\mathcal{G}_0$ [9], [14], [15], generalized gamma (GΓD) [16], [17], Stable-Rayleigh [2], [18], generalised-Gaussian Rayleigh [3].

Combining the Rician idea with the non-Gaussian and heavy-tailed case via the Laplace distribution in [19], [20] addresses both the non-Rayleigh and heavy-tailed characteristics of amplitude SAR images. The Laplace-Rician model, despite being limited to a Laplace distribution as the back-scattered SAR signal components' statistical model, showed superior performance in modeling amplitude SAR images of the sea surface [19], and for some other scenes such as forest, agricultural [20] when compared to state-of-the-art statistical models such as Weibull, lognormal, and $\mathcal{K}$.

In a recent study [21], we have extended the Laplace-Rician model by proposing a much more general case, where the back-scattered SAR signal components are *non-zero mean Generalized-Gaussian* distributed. We have demonstrated the modelling capability of the GG-Rician model for amplitude/intensity SAR images for illuminated scenes of urban, agricultural, land cover and sea surface. The results have

This work was supported by the UK Engineering and Physical Sciences Research Council (EPSRC) under grant EP/R009260/1 (AssenSAR).

Oktay Karakuş is with School of Computer Science and Informatics, Cardiff University, Queen's Buildings, 5 The Parade, Roath, Cardiff, CF24 3AA, U.K. (e-mail: KarakusO@cardiff.ac.uk)

Ercan E. Kuruoğlu is with Data Science and Information Technology Center, Tsinghua-Berkeley Shenzhen Institute, China and is on leave from ISTI-CNR, Pisa, Italy. (e-mail: ercan.kuruoglu@isti.cnr.it)

Alin Achim is with the Visual Information Laboratory, University of Bristol, Bristol BS1 5DD, U.K. (e-mail: alin.achim@bristol.ac.uk)

M. A. Altınkaya is with the Department of Electrical-Electronics Engineering, Izmir Institute of Technology, 35430 Izmir, Turkey (e-mail: mustafaaltinkaya@iyte.edu.tr).

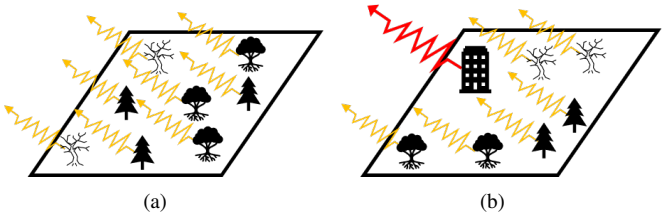

Fig. 1. Surface scattering examples. (a) Distributed scattering, (b) Dominating scatterer + multiple distributed ones.

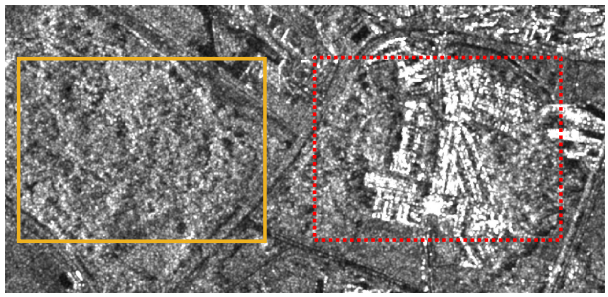

Fig. 2. Real SAR example. Rectangle (left): distributed scattering. (right): a number of strong scatterers.

demonstrated the superior performance and flexibility of the GG-Rician model for all frequency bands and scenes, and its applicability on both amplitude and intensity SAR images.

Despite the successful performance of the previously proposed GG-Rician (incl. Laplace-Rician) distributions in seven different classes of SAR scenes (sea, agricultural, mixed, etc.) in [19]–[21], we have experienced that GG-Rician's modelling performance can be comparable to, and sometimes lower than the GΓD and $\mathcal{G}_0$ models specifically for the urban SAR scenes which include a high number of strong scatterers (such as urban). We believe that heavy-tailed characteristics of the generalised Gaussian family might not be impulsive enough to fully demonstrate scenes with high number of large intensities. Consequently, in this letter, we propose the use of the Cauchy distribution for modelling the backscattered SAR signal real and imaginary components in urban images whilst keeping the Rician base model via non-zero location parameter of the Cauchy density.

A. On the Rician Assumption

As was mentioned in the previous section, the fundamental Rayleigh backscattering idea relies on the assumption that the scene does not have any dominating scatterer whilst having a distributed scattering mechanism. However, in various scenes such as urban ones, the illuminated area may include one (or a small number of) dominating scatterer(s) (Figure 1-(b)), and a large number of non-dominant ones [22]. This phenomenon can also be seen in a real SAR image in Figure 2. The displayed scene within the rectangle on the left is a good example of the distributed scattering whilst radar returns in the rectangle on the right, includes various urban scene targets (buildings, wall corners, etc.). Therefore, the scene on the right includes quite a lot of high intensity returns, resulting in non-distributed scattering. Hence, the assumption on which the Rayleigh backscattering model is based upon would no longer

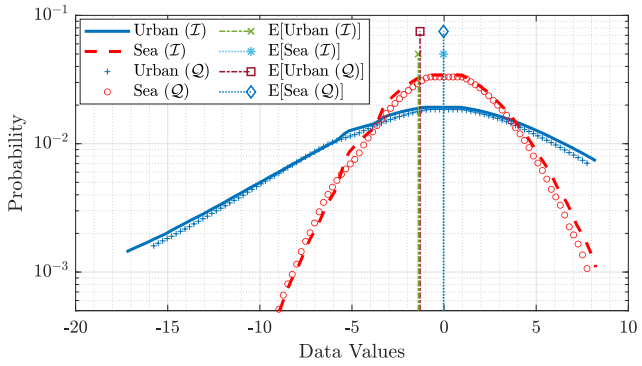

Fig. 3. Comparison for $\mathcal{I}$ and $\mathcal{Q}$ components of different SAR scenes.

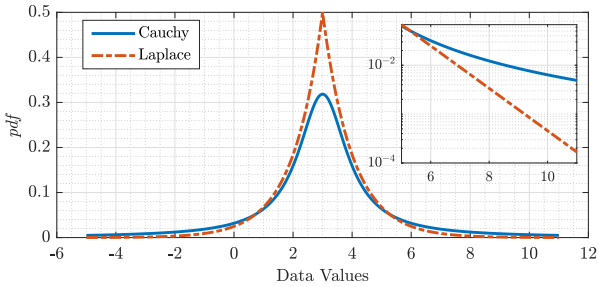

Fig. 4. Laplace *vs.* Cauchy.

be valid. In the statistical point of view, this case results in the signal components x and y still being iid, but this time with non-zero-mean random variables. This statistical case is known to be the Rician backscattering when the signal components are Gaussian.

To prepare a physical base for the Rician assumption in this letter, two different patches (urban and sea surface) from a SAR scene were investigated. The utilised COSMO-SkyMed SAR data incorporates an intensity SAR scene as well as in-phase ($\mathcal{I}$) and quadrature ($\mathcal{Q}$) components of the back-scattered SAR signal. For both urban and sea patches, histograms of $\mathcal{I}$ and $\mathcal{Q}$ components were calculated which are depicted in Figure 3. It is clear from Figure 3 that sea and urban scenes have characteristically different component distributions. Sea surface components are centred around the origin (potentially Rayleigh based) with a mostly symmetric form whilst distributions for urban components are skewed and centred around a "non-zero" data value. This simple example provides a physical support to the use of Rician backscattering specifically for urban SAR scenes.

B. On the Choice of Cauchy Distribution

The Cauchy distribution is known to be heavy-tailed and to promote (statistical) sparsity in various applications. From a purely theoretical viewpoint, our preference for the Cauchy model over other candidate models stems from its membership of the α-Stable family of distributions. Specifically, unlike other empirical distributions able to faithfully fit distributions with heavy-tails, α-stable distributions are motivated by the generalised central limit theorem (CLT) similarly to the way Gaussian distributions are motivated by the classical CLT. Contrary to the general α-stable family, the Cauchy distri-

bution has a closed-form probability density function, which is defined by

$$p(x|\gamma,\delta) = \mathcal{C}a(\delta,\gamma) = \frac{1}{\pi}\frac{\gamma}{\gamma^2+(x-\delta)^2} \tag{2}$$

where γ is the dispersion (scale) parameter, which controls the spread of the distribution, and δ is the location parameter.

Despite the remarkable performance of the Laplace-Rician model [19], [20] in modelling various types of SAR scenes, our motivation is to provide an amplitude model for urban SAR scenes which clearly show heavy-tailed characteristics, since they have more pronounced single reflectors when compared to, for example, sea surface images. Figure 4 compares Laplace and Cauchy distributions whilst their scale and location parameters are the same. It is clear from this visual representation that Laplace pdf is more peaked around the location parameter whilst the Cauchy model has more mass in the tails indicating better potential for modelling impulsive characteristics. It is also interesting to note that the differences between Laplace and Cauchy pdfs in Figure 4 resemble the differences between sea and urban scenes in Figure 3. To this end, Figure 3 also provides support to the need for heavier tailed density for the urban scene modelling.

From another point of view, the need for heavier tailed statistical data models can be modelled with various image processing applications. The Cauchy distributions has been investigated as a statistically sparse statistical model compared to the Laplace in the literature [23]–[25] and provided a remarkable performance in applications such as dictionary learning, despeckling, deblurring.

II. The Cauchy-Rician Density

We first start by assuming that signal components, x_1 and x_2 are non-zero Cauchy distributed as $x_1 \sim \mathcal{C}a(\delta,\gamma)$ and $x_2 \sim \mathcal{C}a(\delta,\gamma)$. Consider the bivariate isotropic Cauchy distribution, the characteristic function of which has the form of $\psi(t_1,t_2) = \exp(j\delta(t_1+t_2) - \gamma|\mathbf{t}|)$, where t_1 and t_2 are components of the vector $\mathbf{t}$, and $|\mathbf{t}|$ is the magnitude. The probability density function (pdf) can be evaluated by taking the 2D Fourier transform as

$$f(x_1,x_2) = \frac{1}{(2\pi)^2}\int_{t_1}\int_{t_2}\exp(j\delta(t_1+t_2))\exp(-\gamma|\mathbf{t}|) \times \exp(-j(x_1t_1+x_2t_2))dt_1dt_2. \tag{3}$$

We make a change of variables and rewrite x_1 and x_2 in terms of variables y_1 and y_2, respectively as $y_1 = x_1 - \delta$, and $y_2 = x_2 - \delta$, which leads to

$$f(y_1+\delta,y_2+\delta) = \frac{1}{(2\pi)^2}\int_{t_1}\int_{t_2}\exp(-\gamma|\mathbf{t}|) \times \exp\{-j[t_1y_1+t_2y_2]\}dt_1dt_2. \tag{4}$$

We now convert this integral into the polar coordinates via $t_1 = u\cos\phi$ and $t_2 = u\sin\phi$

$$f(y_1+\delta_1,y_2+\delta_2) = \int_0^{2\pi}\int_0^{\infty}\frac{u\exp(-\gamma u)}{(2\pi)^2} \times \exp\{-ju[y_1\cos\phi + y_2\sin\phi]\}dud\phi. \tag{5}$$

where $u = |\mathbf{t}|$ and $\phi = \arctan(t_1/t_2)$. If we reorganise (5), $f(y_1+\delta_1, y_2+\delta_2)$ becomes

$$= \frac{1}{2\pi}\int_0^{\infty} u\exp(-\gamma u) \times \left[\frac{1}{2\pi}\int_0^{2\pi}\exp\left(-ju[y_1\cos\phi + y_2\sin\phi]\right)d\phi\right]du. \tag{6}$$

Then, using the identity for the expression in square brackets from [26], we obtain [2]

$$f(y_1+\delta_1,y_2+\delta_2) = \frac{1}{2\pi}\int_0^{\infty} u\exp(-\gamma u^{\alpha})\mathcal{J}_0(u|\mathbf{y}|)du. \tag{7}$$

where $\mathcal{J}_0$ is the zeroth order Bessel function of the first kind. Here, we now have a bivariate density function, and to have amplitude instead of two signal components, we take the following polar transformation

$$f(r,\theta) = rf(y_1+\delta = r\cos\theta, y_2+\delta = r\sin\theta), \tag{8}$$

where $r \geq 0$ and $0 \leq \theta \leq 2\pi$. Then, marginalising over θ leads us to

$$f(r) = \frac{r}{2\pi}\int_0^{2\pi}\int_0^{\infty} u\exp(-\gamma u)\mathcal{J}_0(uA(r,\theta))dud\theta. \tag{9}$$

where $A(r,\theta) = \sqrt{r^2+2\delta^2-2r\delta(\cos\theta+\sin\theta)}$. Reorganising (9), we have

$$f(r) = \frac{r}{2\pi}\int_0^{2\pi} d\theta\int_0^{\infty} u\exp(-\gamma u)\mathcal{J}_0(uA(r,\theta))du. \tag{10}$$

Using the identity below [27]

$$\int_0^{\infty} z^{n+1}\exp(-az)\mathcal{J}_n(bz)dz = \frac{a2^{n+1}b^n\Gamma(n+3/2)}{\sqrt{\pi}(a^2+b^2)^{n+3/2}} \tag{11}$$

where $a > 0$, $b > 0$ and $n > -1$, we rewrite (10) for $n = 0$ as

$$f(r) = \frac{r\gamma}{2\pi}\int_0^{2\pi}\frac{d\theta}{\left[\gamma^2+r^2+2\delta^2-2r\delta(\cos\theta+\sin\theta)\right]^{3/2}} \tag{12}$$

which corresponds to the *Cauchy-Rician* distribution. For $\delta = 0$, it is straightforward to show that the distribution in (12) is simplified to *Cauchy-Rayleigh* distribution of [2] as $f(r) = r\gamma/(r^2+\gamma^2)^{3/2}$. Since the pdf expression in (12) is not in a compact analytical form and it does not seem to be possible to invert it to obtain parameter values, we employ a Bayesian sampling methodology in order to estimate model parameters of γ and δ. We leave the derivation of a closed-form parameter estimation method for future work.

In particular, the method is a Metropolis-Hastings (MH) algorithm, and in each iteration, it applies one of 3 different moves: $\mathcal{M}_1$: Update δ for fixed γ, $\mathcal{M}_2$: Update γ for fixed δ, $\mathcal{M}_3$: Update γ and δ where the probabilities of which are selected as 0.4, 0.4 and 0.2 for $\mathcal{M}_1$, $\mathcal{M}_2$ and $\mathcal{M}_3$, respectively. To test the parameter estimation approach, we create four simulated data sequences and the proposed algorithm was used to estimate δ and γ for each data set. The corresponding data sets (δ,γ) are (2, 2), (4, 0.5), (5, 9) and (40, 15) all of which have 1500 samples.

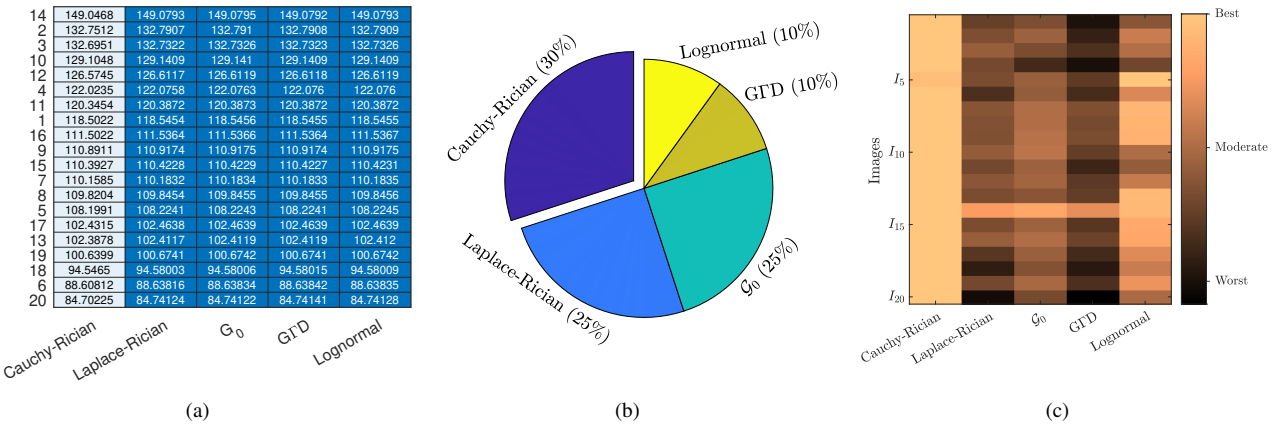

(a) (b) (c)

Fig. 5. Modeling performance analysis in terms of the (a) RSE (each row represents SAR images, I_i), (b) KL-divergence, and (c) AICc.

The modelling results let us conclude that the location parameter δ results are generally close to the real values (e.g. $\delta = 2$ is estimated as 2.011). Overestimation can be seen for the scale parameter γ estimation results (e.g. $\gamma = 0.5$ is estimated as 0.656), however, the statistical significance results show remarkable performance as KL divergence values are relatively small (between 0.038 and 0.057). Furthermore, the estimated parameters are also statistically significant since p-values are greater than 0.9999 for all four data sets.

III. Experimental Results

The proposed method was tested on various urban SAR data. We subsequently conducted experiments to determine the best fitting distribution for given real urban SAR images. In order to measure modelling performance, we used *Kullback-Leibler* (KL) divergence, residual standard error (RSE), the corrected Akaike information criterion (AICc) [28] and log-likelihood (logLHD). The proposed method was tested on 20 different urban SAR images coming from TerraSAR-X, and ICEYE. The performance of the Cauchy-Rician model was compared to Laplace-Rician, Lognormal, $\mathcal{G}_0$, and GΓD distributions. It is worth noting that other common models such as the Rayleigh, Gamma, and $\mathcal{K}$ distributions have been left aside from our simulations, since our previous work have shown that they are less successful than the utilised reference models [21]. The results are depicted in Figures 5 and 6, and Table I.

Evaluating the sub-figures in Figure 5, in terms of the KL divergence results for overall percentages, even though the proposed model is the best model for 30% of the total 20 SAR scenes, $\mathcal{G}_0$ and Laplace-Rician models also perform similar to the Cauchy-Rician. The superiority of the proposed method can been seen from the RSE and AICc sub-figures. The Cauchy-Rician model is the best model for all urban SAR scenes in terms of the RSE and AICc values.

Figure 6 presents SAR images for two example urban scenes and their modeling results in logarithmic scale. The log-scale pdf modeling results in Figure 6 (c)-(f) confirm the numerical results presented in Figure 5. Despite having slightly over-estimates around the peak of the histogram, the Cauchy-Rician specifically outperforms most of the reference models utilised in this study with its strong tail modelling capability.

In order to quantitatively support the tail modelling performance of the Cauchy-Rician model, we also performed a simulation case for only the tails of the image histograms for $CDF(I_i) \geq 0.75$ and $CDF(I_i) \geq 0.90$. In order to measure how informative the tail modelling is, we used negative log-likelihood ratio ($-\log$LHD) and decided the best model which minimises $-\log$LHD. Table I presents the percentages of SAR scenes for two different analyses. It is clear from the table that the proposed Cauchy-Rician density performs better tail modelling compared to state-of-the-art models such as $\mathcal{G}_0$, and GΓD despite having only two model parameters. Figure 6 (e)-(f) also provide visual demonstrations of the tail modelling performance.

TABLE I
Tail Modeling Analysis

Tail samples	Cauchy *Rician*	Laplace *Rician*	$\mathcal{G}_0$	GΓD	*Lognormal*
$CDF(I_i) \geq 0.75$	**35%**	0%	30%	15%	20%
$CDF(I_i) \geq 0.90$	**95%**	0%	5%	0%	0%

IV. Conclusion

This letter introduced the Cauchy-Rician distribution to characterise the amplitude of the complex back-scattered SAR signal from urban scenes. Following the theoretical and physical aspects of the urban SAR scenes, the proposed approach leveraged both heavy-tailed distributions and the Rician back-scattering. Thanks to Cauchy distribution's ability to model heavy-tails, the proposed model further extended the idea behind GG-Rician density [21] for SAR scenes that require heavier tails than that of GG-Rician. Despite having only two model parameters and exploiting only one member of α-Stable distributions, the Cauchy-Rician density demonstrated considerable improvement in performance compared to the state-of-the-art advanced models such as $\mathcal{G}_0$ and GΓD.

References

[1] J. M. Nicolas and F. Tupin, "A new parameterization for the Rician distribution," *IEEE Geoscience and Remote Sensing Letters*, vol. 17, no. 11, pp. 2011–2015, 2020.

[2] E. E. Kuruoglu and J. Zerubia, "Modeling SAR images with a generalization of the Rayleigh distribution," *IEEE Transactions on Image Processing*, vol. 13, no. 4, pp. 527–533, 2004.

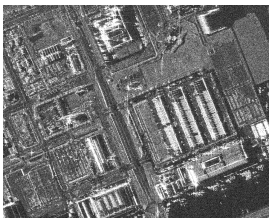

(a) I_{12}

(b) I_{16}

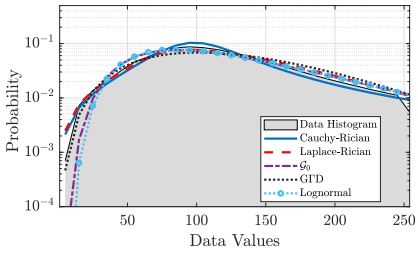

(c) log-*pdf*

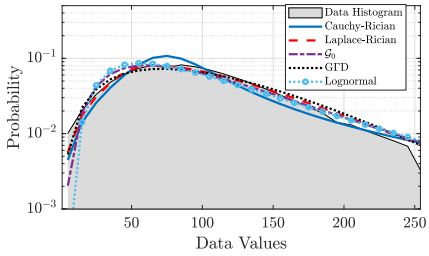

(d) log-*pdf*

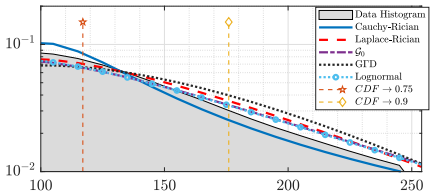

(e) log-*pdf* (tails)

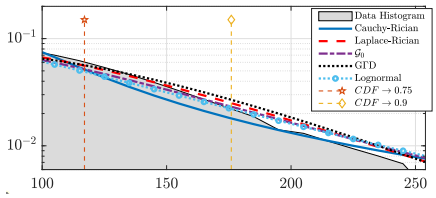

(f) log-*pdf* (tails)

Fig. 6. Visual evaluation of SAR amplitude models.

[3] G. Moser, J. Zerubia, and S. B. Serpico, "SAR amplitude probability density function estimation based on a generalized Gaussian model," *IEEE Transactions on Image Processing*, vol. 15, no. 6, pp. 1429–1442, 2006.

[4] J. W. Goodman, "Statistical properties of laser speckle patterns," in *Laser speckle and related phenomena*. Springer, 1975, pp. 9–75.

[5] T. Eltoft, "The Rician inverse Gaussian distribution: a new model for non-Rayleigh signal amplitude statistics," *IEEE Transactions on Image Processing*, vol. 14, no. 11, pp. 1722–1735, 2005.

[6] G. Gao, "Statistical modeling of SAR images: A survey," *Sensors*, vol. 10, no. 1, pp. 775–795, 2010.

[7] W. Wu, H. Guo, and X. Li, "Man-made target detection in urban areas based on a new azimuth stationarity extraction method," *IEEE Journal of Selected Topics in Applied Earth Observations and Remote Sensing*, vol. 6, no. 3, pp. 1138–1146, 2013.

[8] J. Sun, X. Wang, X. Yuan, Q. Zhang, C. Guan, and A. V. Babanin, "The Dependence of Sea SAR Image Distribution Parameters on Surface Wave Characteristics," *Remote Sensing*, vol. 10, no. 11, p. 1843, 2018.

[9] S. Cui, G. Schwarz, and M. Datcu, "A comparative study of statistical models for multilook sar images," *IEEE Geoscience and Remote Sensing Letters*, vol. 11, no. 10, pp. 1752–1756, 2014.

[10] S. Chitroub, A. Houacine, and B. Sansal, "Statistical characterisation and modelling of SAR images," *Signal Processing*, vol. 82, no. 1, pp. 69–92, 2002.

[11] J. R. M. Fernández, "Estimation of the relation between Weibull sea clutter and the CA-CFAR scale factor," *Revista Ingeniería*, vol. 25, no. 2, pp. 19–28, 2015.

[12] Z. Chen, X. Liu, Z. Wu, and X. Wang, "The Analysis of Sea Clutter Statistics Characteristics Based on the Observed Sea Clutter of Ku-Band Radar," in *2013 Proceedings of the International Symposium on Antennas & Propagation*, vol. 2. IEEE, 2013, pp. 1183–1186.

[13] M. Migliaccio, L. Huang, and A. Buono, "Sar speckle dependence on ocean surface wind field," *IEEE Transactions on Geoscience and Remote Sensing*, vol. 57, no. 8, pp. 5447–5455, 2019.

[14] A. C. Frery, H.-J. Muller, C. d. C. F. Yanasse, and S. J. S. Sant'Anna, "A model for extremely heterogeneous clutter," *IEEE transactions on geoscience and remote sensing*, vol. 35, no. 3, pp. 648–659, 1997.

[15] S. Cui and M. Datcu, "Coarse to fine patches-based multitemporal analysis of very high resolution satellite images," in *2011 6th International Workshop on the Analysis of Multi-Temporal Remote Sensing Images (Multi-Temp)*. IEEE, 2011, pp. 85–88.

[16] E. W. Stacy *et al.*, "A generalization of the gamma distribution," *The Annals of mathematical statistics*, vol. 33, no. 3, pp. 1187–1192, 1962.

[17] H.-C. Li, W. Hong, Y.-R. Wu, and P.-Z. Fan, "On the empirical-statistical modeling of sar images with generalized gamma distribution," *IEEE Journal of selected topics in signal processing*, vol. 5, no. 3, pp. 386–397, 2011.

[18] O. Karakuş, E. E. Kuruoğlu, and M. A. Altınkaya, "Generalized Bayesian model selection for speckle on remote sensing images," *IEEE Transactions on Image Processing*, vol. 28, no. 4, pp. 1748–1758, 2018.

[19] O. Karakuş, E. E. Kuruoğlu, and A. Achim, "Modelling sea clutter in SAR images using Laplace-Rician distribution," in *ICASSP 2020 - 2020 IEEE International Conference on Acoustics, Speech and Signal Processing (ICASSP)*, 2020, pp. 1454–1458.

[20] O. Karakus, E. E. Kuruoglu, and A. Achim, "A Modification of Rician Distribution for SAR Image Modelling," in *EUSAR 2021; 13th European Conference on Synthetic Aperture Radar*. VDE, 2021, pp. 1–6.

[21] O. Karakuş, E. E. Kuruoğlu, and A. Achim, "A generalized Gaussian extension to the Rician distribution for SAR image modeling," *IEEE Transactions on Geoscience and Remote Sensing*, 2021.

[22] D. Yue, F. Xu, A. C. Frery, and Y. Jin, "SAR image statistical modeling : Part one–single-pixel statistical models," *IEEE Geoscience and Remote Sensing Magazine*, pp. 0–0, 2020.

[23] O. Karakuş, P. Mayo, and A. Achim, "Convergence guarantees for non-convex optimisation with cauchy-based penalties," *IEEE Transactions on Signal Processing*, vol. 68, pp. 6159–6170, 2020.

[24] O. Karakuş and A. Achim, "On solving sar imaging inverse problems using nonconvex regularization with a cauchy-based penalty," *IEEE Transactions on Geoscience and Remote Sensing*, 2020.

[25] P. Mayo, O. Karakuş, R. Holmes, and A. Achim, "Representation Learning via Cauchy Convolutional Sparse Coding," *IEEE Access*, vol. 9, pp. 100 447–100 459, 2021.

[26] M. Abramowitz and I. A. Stegun, *Handbook of mathematical functions: with formulas, graphs, and mathematical tables*. Courier Corporation, 1965, vol. 55.

[27] I. S. Gradshteyn and I. M. Ryzhik, *Table of integrals, series, and products*. Academic press, 2014.

[28] J. E. Cavanaugh and A. A. Neath, "The Akaike information criterion: Background, derivation, properties, application, interpretation, and refinements," *Wiley Interdisciplinary Reviews: Computational Statistics*, vol. 11, no. 3, p. e1460, 2019.